**A&A manuscript no.**
(will be inserted by hand later)

**Your thesaurus codes are:**
**08((08.01.1), (08.03.5), (08.09.2) AB Dor, (08.12.1), (08.16.5), (13.21.5), (13.25.5))**

ASTRONOMY
AND
ASTROPHYSICS
16.4.1996

# Simultaneous EUVE & ASCA observations of AB Dor:

## Temperature structure & abundances of the quiescent corona

**R. Mewe**[1], **J.S. Kaastra**[1], **S.M. White**[2], **and R. Pallavicini**[3]

[1] SRON Laboratory for Space Research, Sorbonnelaan 2, NL-3584 CA Utrecht, The Netherlands
[2] Department of Astronomy, University of Maryland, College Park, MD 20742, USA
[3] Osservatorio Astronomico "G.S. Vaiana", Piazza del Parlamento 1, I-90134 Palermo, Italy

Received date ...; accepted date ...

**Abstract.** We have analyzed EUV and X-ray spectra of the non-flaring state of AB Dor, obtained from simultaneous observations with EUVE and ASCA. The coronal temperature structure and the coronal elemental abundances have been derived by jointly fitting the spectra, including lines and continuum. We have applied a multi–temperature fitting method and we have found that an optically thin plasma model with *solar abundances* (relative to hydrogen) does not yield a good fit. A 4-T fit allowing the abundances of the more important elements (Fe, S, Si, Mg, Ne, and O) plus four other less important abundances (N, Ar, Ca, and Ni) to vary improves the fit markedly. This results in values of the first 6 abundances relative to solar photospheric values that are significantly (a factor 2–3) below solar except for Ne, which is solar, while most of the remaining four abundances are consistent both with solar and reduced abundances. In the course of the 4-T fitting we have determined a best-fit value for the interstellar hydrogen column density of $N_{\rm H}$ = (2.0 ± 0.5) $10^{18}$ cm$^{-2}$. We have applied four differential emission measure (DEM) distribution analysis techniques, *viz.*: (i) regularization method, (ii) polynomial method, (iii) clean algorithm, and (iv) genetic algorithm. The four different methods all yield a qualitatively similar DEM, showing two maxima in the temperature intervals 5–8 MK and 20–30 MK. Our analysis demonstrates the great value of simultaneous ASCA and EUVE observations in determining the fundamental parameters of stellar coronae.

**Key words:** stars: coronae - activity - late-type - pre-main-sequence - abundances - AB Dor - ultraviolet: stars - X-rays: stars

*Send offprint requests to*: R. Mewe

## 1. Introduction

AB Doradus (HD 36705, spectral type K0-2 IV-V) is one of the most interesting, and most intensively studied, coronal X-ray sources. It has attracted attention for a number of reasons. First, it is one of the most rapidly rotating effectively single stars known, with a period of only 12.4 hours, and it is relatively close, at a distance of about 15 pc (Guirado et al. 1995). Further, it is a very young star with a strong lithium absorption line (Rucinski 1985, Vilhu et al. 1987) and kinematic properties characteristic of the Pleiades moving group (Innis et al. 1986). This makes it probably the nearest pre-main-sequence star known, with an age of only $\lesssim$ 50 Myr; its proximity makes it an easy-to-study analogue of the numerous rapidly rotating dwarf stars in the Pleiades open cluster and in star forming regions.

Attention was first drawn to this southern star by Pakull (1981) who identified it with a flaring X-ray source detected by the *Einstein* Observatory, and carried out photometry which indicated the presence of spots and a rotation period of only half a day. Both quiescent and flaring X-ray emission have been further studied by Collier Cameron et al. (1988) using EXOSAT and by Vilhu et al. (1991) using GINGA. Rucinski (1985) studied AB Dor with IUE and found some evidence for rotational modulation of the transition-region lines. Lim et al. (1992) found the presence of rotational modulation in the radio emission which led to an estimate of the size of the emitting structures. AB Dor has been extensively observed with ROSAT (e.g., Kürster and Dennerl 1993, Kürster 1995).

Optical photometry indicates large and long-lived starspots which tend to form at two opposite longitude zones (Innis et al. 1986). The rotation axis of AB Dor is thought to be inclined at an angle of 60° to the line of sight (Kürster et al. 1994), so only a region near one pole is visible all the time. If rotational modulation is present, this means that active regions at low latitudes have a highly inhomogeneous distribution, as could be expected from dynamo-generated magnetic activity. Kürster et al. (1992, 1994) have reconstructed the distribution of spots over the surface of AB Dor from high-resolution optical spectra and Doppler imaging techniques. H$\alpha$ spectroscopy showed remarkable features: transients moving at high velocity with respect to the star, which may represent evidence for mass loss in the form of large discrete events in the corona (Collier Cameron & Robinson 1989). In brief, AB Dor is an ideal object to study dynamo-generated magnetic activity in a young star. In addition, it offers a means to infer the properties of the Sun during its pre-main sequence evolution, since the Sun must have been very similar to AB Dor at an age of $\sim$ 50 Myr.

A differential emission measure (DEM) analysis of the EUVE spectrum of AB Dor has shown that if we assume *solar photospheric* abundances, the *formal* DEM solution requires a very hot component ($\gtrsim$3 $10^7$ K) to explain the low line-to-continuum ratio in the SW band between 80–150 Å (Rucinski et al. 1995). We have encountered the same problem in the analysis of the EUVE spectra of several other cool stars and we have discussed a number of possible reasons for this, such as improper background subtraction, resonant line scattering, reduced abundances, optically thick continuum, or a real hot plasma component (e.g., Mewe et al. 1995b, Schrijver et al. 1995). However, in the case of AB Dor there is direct evidence against the existence of such a very hot component in the corona: ASCA data taken at the same time in the range 0.5–10 keV, where such a component should radiate most strongly, show no evidence for it (White et al. 1996b,c). In the case of the EUVE spectrum, the hot component in the DEM is no longer required by the fits to the spectrum if the Fe abundance is taken to be sufficiently low (about 1/3 solar). This factor is consistent with the low Fe abundance derived independently from a two-temperature analysis of the quiescent ASCA spectrum of AB Dor (White et al. 1996b,c), but is difficult to explain in a young PMS star whose photospheric "metal" abundances are solar (Vilhu et al. 1987). The reduced coronal Fe abundance is also at variance with the "FIP effect" observed in solar coronal spectra: there Fe, with its low first ionization potential (FIP), is enhanced with respect to photospheric values (e.g., Meyer 1991, Feldman 1992). This makes the abundances as recently reported by ASCA for several coronal sources rather intriguing (cf. White et al. 1994, Drake et al. 1994, White 1996). As has been widely recognized, ASCA and EUVE datasets are highly complementary: both sample coronal temperatures, but while the EUVE spectral range is dominated by many Fe lines from different charge states, the ASCA spectral range is dominated by hydrogen (and helium) continuum as well as lines from many more elements, but with each contributing from fewer charge states. Thus EUVE is excellent for determining DEMs, while ASCA data only poorly constrain more than two temperature components but are excellent for determining abundances. As we show here, the combination of the two is very powerful and eliminates many of the ambiguities inherent to the use of data from one or other satellite alone (uncertain abundances in the case of EUVE, poorly constrained DEM in the case of ASCA). In the present paper we analyze simultaneous EUVE & (quiescent) ASCA data to derive DEM distributions and coronal elemental abundances for AB Dor (preliminary results were reported by Mewe et al. 1996a).

## 2. Observations

AB Dor was observed by EUVE on 1993 November 4–11 (JD 2449295.94–2449302.74), covering 14 rotations of the star (Rucinski et al. 1995; the reduction of the EUVE data is discussed in this paper). The total effective observing time was 1.49 $10^5$ s. The data were collected in three spectroscopic bands, SW (80–180 Å), MW (150–350 Å), and LW (300–700 Å) with spectral resolutions of 0.5, 1, and 2 Å, respectively. During these observations AB Dor did not show any major flaring in the EUV, while optical monitoring showed no flaring except during a brief period amounting to no more than 5% of the EUVE observation (White et al. 1996a). Therefore we assume that our EUVE spectrum is representative for the quiescent state of AB Dor. Within the EUVE exposure, ASCA has observed AB Dor on 1993 November 7–8 (White et al. 1996b,c). We use the data from the SIS0 detector obtained during the quiescent period which occurred during the first 6 hours of the observation from 1993 Nov 7 13:00–19:00 UT; thereafter a succession of flares dominates the remaining time (for more details, see White et al. 1996b). The effective observation time was 1.77 $10^4$ s. and the total counting rate integrated over the whole spectral band (0.38–8.68 keV) was 1.36 $\pm$ 0.01 c/s, resulting in a spectrum with excellent signal–to–noise. The ASCA data were reduced in the *ftools* package and background–subtracted following standard procedures. Both the raw EUVE spectrum and the raw ASCA spectrum have many more spectral bins than the spectral resolution of the instruments merit. Consequently, the spectra were rebinned into 463 (EUVE) + 147 (ASCA SIS0) = 610 energy bins, with a corresponding improvement in photon statistics. In the ASCA data we included a systematic error of 2 % of the source flux, in order to account for systematic errors in both the data and the spectral model. There is additional uncertainty at lower energies due to calibration uncertainties and therefore we have taken a systematic error of 5 % below 0.8 keV. For EUVE we have introduced systematic errors of 15 % for both source and background (cf. Rucinski et al. 1995).

## 3. Spectral model

We calculate collisional ionization equilibrium spectra using a spectral code which has evolved from the well–known optically–thin plasma code developed by Mewe and co–workers (e.g., Mewe et al. 1985, 1986). The updated code (cf. Kaastra and Mewe 1993, Mewe and Kaastra 1994, Mewe et al. 1995a) includes improved results for the Fe L-shell complex around 1 keV (Liedahl et al. 1995); it is augmented with spectral lines between 300–2000 Å from Landini and Monsignori Fossi (1990) but with wavelengths and excitation rates modified in several places; the emissivities of about 500 Fe VIII–XVI lines between 35–1960 Å were (re)calculated. The treatment of the continuum emission has also been improved, using photo-ionization rates based upon Verner and Yakovlev (1995). The plasma code is incorporated in the SPEX code (Kaastra et al. 1996b). We include the interstellar absorption using the Morrison and McCammon (1983) model, and determine it as part of the solution in our multi-temperature fit. We adopt a source distance for AB Dor of $d = 15$ pc based on the recent VLBI determination by Guirado et al. (1995); note that previously the distance was thought to be 25 pc. Solar photospheric abundances are taken from Anders and Grevesse (1989).

## 4. DEM analysis methods

Stellar coronae, which are assumed to be optically thin at the wavelengths of interest, are highly structured by stellar magnetic fields. The weak nature of cross–field diffusion of heat allows different field lines to be at different temperatures, and consequently the corona is not well represented by a single temperature. Plasma at many different temperatures will contribute to the X–ray/EUV spectrum. In order to investigate the temperature structure in detail, we have developed various methods to analyze the emission measure distribution with continuous models. These methods use a pre-calculated set of model spectra $\mathbf{f}(\lambda_{\rm i}, {\rm T_j})$, i.e., the plasma emissivity per unit $n_e n_H$ (product of electron and hydrogen density) for an electron temperature grid $\rm T_j$. These spectra are folded through the instrument response, include interstellar absorption and take into account the appropriate abundances. We introduce the "differential emission measure" (DEM) distribution which is defined to be $\mathbf{D}({\rm T}) = n_{\rm e} n_{\rm H} dV/d\log{\rm T}$ ($V$ the emitting plasma volume). It is the weighting function which measures how strongly any particular temperature contributes to the observed spectrum. The DEM distribution is derived by matching the observed (wavelength) spectrum $\tilde{\mathbf{g}}(\lambda_{\rm i})$ as good as possible to the model spectrum $\mathbf{g}(\lambda_{\rm i})$ for a grid of temperatures ranging from $\rm T_1$ up to $\rm T_M$:

$$\mathbf{g}(\lambda_{\rm i}) = \int \mathbf{f}(\lambda_{\rm i}, {\rm T}) n_{\rm e}({\rm T}) n_H({\rm T}) dV({\rm T}) \simeq \sum_{\rm j=1}^{M} \mathbf{f}(\lambda_{\rm i}, {\rm T_j}) \mathbf{D}({\rm T_j}) \Delta \log({\rm T_j}). \quad (1)$$

It is important to include the continuum in the analysis since the line–to–continuum ratio contains important information on the abundances (in particular the [Fe/H] ratio) and line scattering effects. For many active stars with hot coronae dominated by Fe lines, the line–to–continuum ratio is the *only* abundance diagnostic in an EUVE spectrum. The interpretation of the line–to–continuum ratio in EUVE SW spectra has been controversial, with opinions differing on the possible role of scattering optical depth and on unresolved lines contributing to an "apparent" continuum. In the data analysis we initially proceed by ignoring such possible effects, deferring discussion to the last section.

The wavelength range covered by EUVE has many lines sensitive to temperatures below 2 $10^7$ K but contains only a few weak lines from plasma at temperatures exceeding about 2 $10^7$ K. Thus only the EUV continuum is sensitive to this hot temperature range, but the *shape* of the continuum emission component in the EUVE range is rather insensitive to changes in the temperature for $\rm T \gtrsim 3\ 10^6$ K. Thus the hotter temperatures in our grid are poorly constrained in the EUVE spectrum. On the other hand, the ASCA spectrum contains many strong temperature–constraining lines from plasma with $\rm T \gtrsim 10^7$ K. Thus we have sufficient constraints on the DEM in the entire temperature range of our grid.

The two instruments cover a total range of about 0.01–10 keV. Therefore we use in the DEM modeling a logarithmically spaced grid of 31 temperatures between 0.01–10 keV (1.16 $10^5$ – 1.16 $10^8$ K) with a step of $\Delta\log{\rm T} = 0.1$ (about 1/3 of the effective temperature resolution). The emission measure is plotted as $\mathbf{D}({\rm T})\Delta\log{\rm T}$ so that the total emission measure in any temperature range can be obtained by summing the values of $\mathbf{D}({\rm T})\Delta\log{\rm T}$ in the relevant temperature bins. We use the $\chi^2$ statistic as a measure of quality of the fit.

Below we briefly mention the five methods that we have applied in our analysis: (i) multi–temperature fitting, (ii) regularization method, (iii) polynomial method, (iv) clean algorithm, and (v) genetic algorithm. The first, fourth and fifth methods are more suited to resolve discrete narrow temperature structures, whereas the second and third methods are more suited for for smooth temperature distributions. For a detailed description we refer to Kaastra et al. (1996a).

### *4.1. Multi–temperature fitting*

We use as the first method a multi-temperature fitting technique which can be considered as a DEM method using as basic functions delta–functions in temperature (compare, for example, the polynomial method which uses Chebyshev polynomials as basic functions). Multi–temperature fitting has been applied many times in analyzing the X–ray spectra of stellar coronae (e.g., Swank et al. 1981).

### *4.2. Regularization method*

This method is treated in detail by Mewe et al. (1995b, 1996b), but see the discussions by Kaastra et al. (1996a). It uses direct matrix inversion of Eq. (1) with the additional constraint that the $2^{\rm nd}$-order derivative of the solution $\mathbf{D}(\mathrm{T})\Delta\log\mathrm{T}$ is as smooth as statistically allowed by the data. This smoothing damps unphysical oscillations which otherwise occur because the data contain noise. The degree of smoothing is controlled by a regularization parameter which is essentially a measure of the relative weight of the smoothness constraint with respect to the $\chi^2$-minimization constraint. For further details about choosing the regularization parameter we refer to Kaastra et al. (1996).

The regularization method works optimal for smooth, continuous temperature distributions. However simulations show that it can also find more discrete temperature structures, although it can never resolve them better than to within a factor of $\sim$2. A drawback of the regularization method is that it cannot prevent the solution from taking negative values at some temperatures, but it is possible to develop some criterion to weigh how much positivity is violated (cf. Kaastra et al. 1996a).

### *4.3. Polynomial method*

A second approach that is also useful for smooth emission measure distributions is an iterative polynomial method, which was applied before to e.g. EXOSAT data (Lemen et al. 1989) and EUVE data (Stern et al. 1995). The shape of $\mathbf{D}(\mathrm{T})$ is approximated by the exponential of a polynomial and we write:

$$\log[\mathbf{D}(\mathrm{T})\Delta\log(\mathrm{T})] = \sum_{\mathrm{k}=0}^{\mathrm{N}-1} a_{\mathrm{k}} P_{\mathrm{k}}(\log\mathrm{T}), \qquad (2)$$

where $P_{\mathrm{k}}$ is a Chebyshev polynomial of order k. This ensures that the coefficients, $a_{\mathrm{k}}$, are all roughly the same order of magnitude and makes the search for the best solution over parameter space better conditioned. In this way it is also ensured that the emission measure distribution is positive for all temperatures, and that low and high temperatures have the same relative resolution. Eq. (2) allows any arbitrary functional form for the DEM to be approximated as the number of terms in the sum is increased. In principle, one should choose solutions with the lowest order polynomial which still provides an acceptable fit to the data. It turns out that for $\mathrm{N} \gtrsim 10$ the fit does no longer improve significantly so that generally $\mathrm{N} \simeq 10$ appears to be an optimal choice.

### *4.4. Clean algorithm*

The clean algorithm (Högbom 1974) is a powerful tool developed originally for the analysis of radio interferometer data.

In an iterative procedure, isothermal spectra are subtracted from the observed spectra until only noise is left. In that case the corresponding $\chi^2$ no longer significantly decreases and the accumulated DEM is the final solution. Simulations have shown that this method is very fast and powerful for discrete temperature structures. This method precludes negative values for the DEM. For more details, see Kaastra et al. (1996a).

### *4.5. Genetic algorithm*

Genetic algorithms (Charbonneau 1995) are based on the biological notion of evolution by means of natural selection. They use an initial population of randomly chosen solutions. Each solution is assigned a "fitness". By breeding this population, using crossover and mutation of the genes of the individuals, the population gradually evolves towards a solution with higher fitness. In the implementation of the method, an individual of the population corresponds to a DEM distribution. The "genes" of each individual consist of the values of the emission measure at the given temperature grid. For the fitness of an individual we take minus the $\chi^2$-statistic of the corresponding model spectrum as compared to the observed spectrum; thus increasing fitness means decreasing $\chi^2$. We start with a population of 1024 individuals. The method precludes negative DEM values. For reference and details, see Kaastra et al. (1996a).

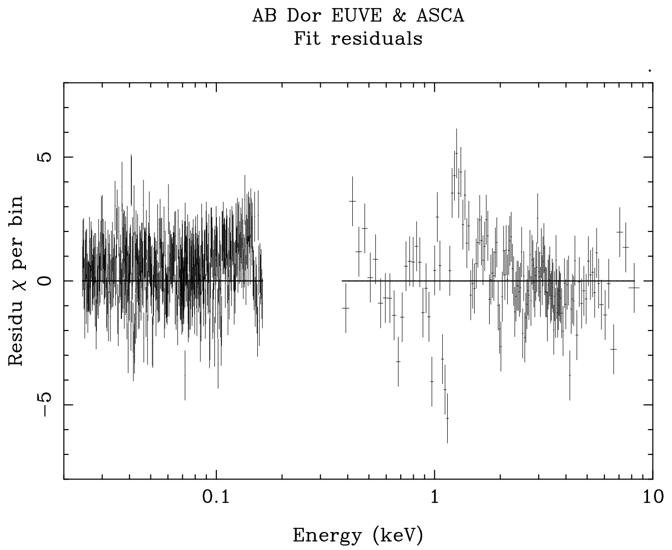


**Fig. 1.** Fit residuals of the combined EUVE & ASCA spectra of AB Dor using a 4-temperature fit method with solar abundances. Error bars indicate $\pm1\sigma$ errors like in all other figures.

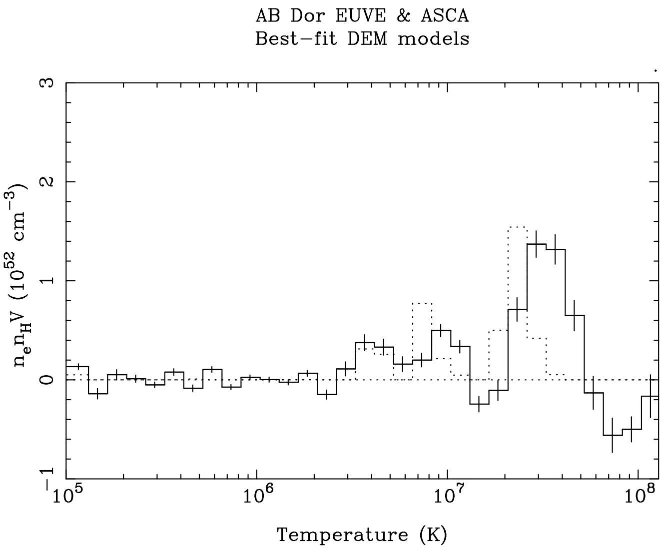


**Fig. 2.** The DEM for the combined EUVE & ASCA data using the regularization method (solid line with $\pm 1\sigma$ error bars) or the clean method (dotted line) with solar abundances.

## 5. Results

### *5.1. Solar abundances*

We start by performing multi-temperature fits. Initially we fix the abundances at solar photospheric abundances (Anders and Grevesse 1989), and adopt a value of $2\ 10^{18}$ cm$^{-2}$ for $N_{\rm H}$ (cf. Sec. 5.2.). It turns out that a two– or three–temperature model is not sufficient to fit all lines in the two spectra, especially the He II 304 Å line. We need a fourth low-temperature component to make a *formal* fit to the latter line. However, even with four temperature components the model gives a very poor fit: $\chi^2$ = 1238 for 602 degrees of freedom (dof). The fit residuals (Fig. 1) are large (up to $\sim 5\sigma$), especially in the ASCA spectral region, and there is evidence for systematic tendencies, in the sense that the fit residuals are systematically above or below zero in certain energy ranges rather than being randomly distributed.

As an illustration of the DEM analysis we show in Fig. 2 the results for the DEM obtained with the regularization method ($\chi^2$ = 1284 for 579 dof with 31 temperature intervals) and the clean method ($\chi^2$ = 1495 for 579 dof). A striking feature of the solution for the regularization method is the presence of significant *negative* excursions in the DEM, especially above about 5 $10^7$ K, which do not show up in the DEM obtained with the clean method. As noted before the regularization method does not prevent $\mathbf{D}$(T) from taking negative values, whereas in the clean method the DEM is forced to positive values. The strong negative excursions in the DEM allow a somewhat better fit in a statistical sense, but at the same time clearly indicate that something is wrong with either the model, the instrumental calibration, or the observations. Negative excursions may still be present in a physically meaningful fit, but should mostly be statistically consistent with zero, or else compensated by neighbouring positive values such that the application of stronger regularization constraints will remove the negative values (effectively smoothing them out).

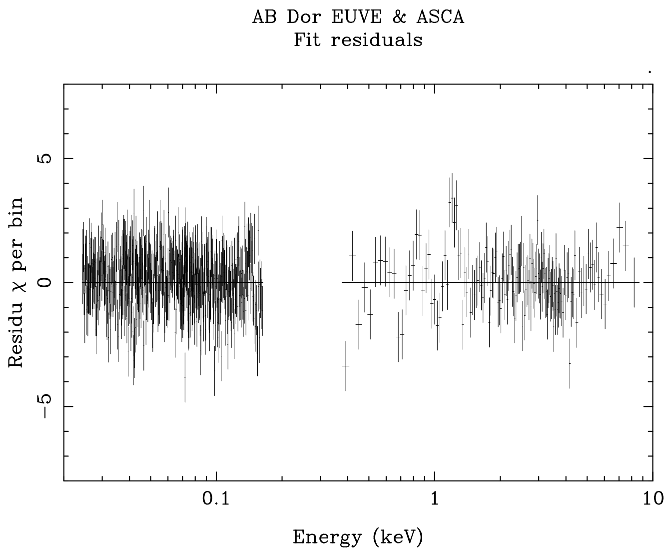


**Fig. 3.** Fit residuals of a 4-T fit to the combined EUVE & ASCA spectra of AB Dor with varied abundances (Table 1).

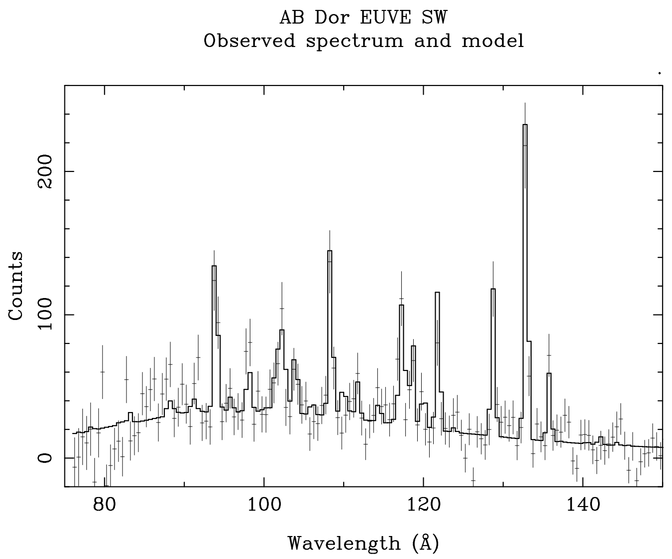


**Fig. 4.** Observed and fitted EUVE SW spectrum of AB Dor for a 4-T fit applied to EUVE/ASCA data with abundances from Table 1.

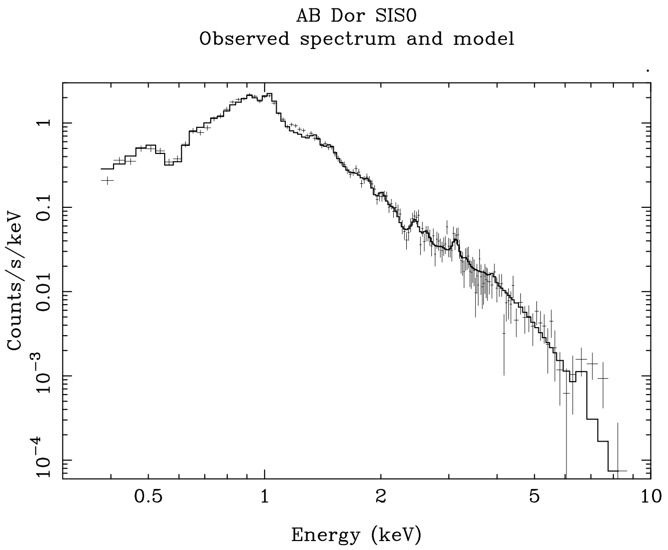


**Fig. 5.** Observed and fitted ASCA spectrum of AB Dor for a 4-T fit applied to EUVE/ASCA data with abundances from Table 1.

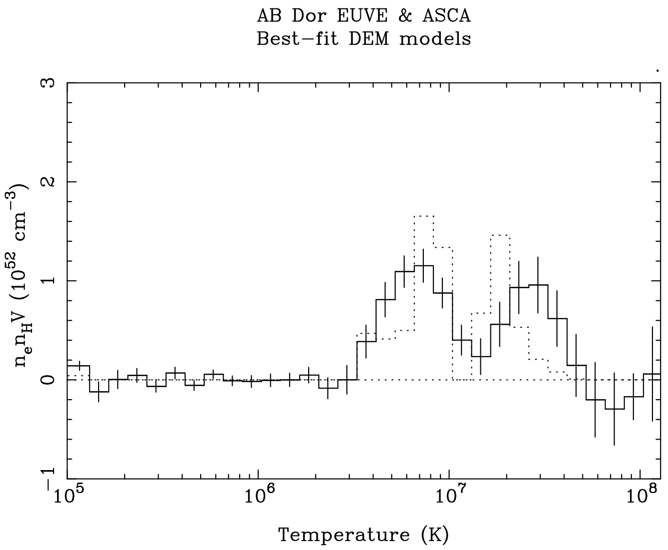


**Fig. 6.** The DEM for the combined EUVE & ASCA data using the regularization method (solid line with error bars) or the clean method (dotted line) with abundances from Table 1.

### *5.2. Non-solar abundances*

Elements for which strong, isolated lines are present in the spectrum yield the most reliable abundances. This is the case for the elements Fe, S, Si, Mg, Ne, and O. The Fe abundance is most accurately determined and is constrained by the ASCA spectrum (Fe L-shell $\sim 1$ keV complex and 6.7 keV Fe K-shell feature) and by the line/continuum ratio in the EUVE SW band. The abundances of Si and S are predominantly determined from the He- and H-like line complexes at $\sim 1.9$ and $\sim 2.5$ keV, respectively. The O abundance is mainly derived from the 0.65 keV Lyman $\alpha$ line, which is however partly blended by the Fe L complex. The Mg abundance is essentially based on the He- and H-like line complex at $\sim 1.4$ keV. The Ne abundance is derived from the 0.92 keV Ne IX and 1.02 keV Ne X lines, which however are just in the middle of the Fe L feature, but the Ne VII/VIII line blend at 88 Å and the Ne VIII line at 98 Å in the EUVE SW spectrum help to constrain the Ne abundance.

**Table 1.** Coronal abundances for AB Dor relative to solar photospheric

| Well constrained | | Poorly constrained | |
|---|---|---|---|
| Element | Abundance | Element | Abundance |
| O | $0.42 \pm 0.08$ | N | $< 0.35$ |
| Ne | $1.20 \pm 0.15$ | Ar | $0.98 \pm 0.47$ |
| Mg | $0.58 \pm 0.10$ | Ca | $0.49 \pm 0.43$ |
| Si | $0.35 \pm 0.08$ | Ni | $0.45 \pm 0.25$ |
| S | $0.37 \pm 0.14$ | | |
| Fe | $0.23 \pm 0.02$ | | |

Again we perform a 4–temperature fit. If we allow the abundances of the six elements which are most sensitive to abundance variations in the spectrum (O, Ne, Mg, Si, S, and Fe) plus four other less important abundances (N, Ar, Ca, and Ni) to vary, the fit improves significantly: $\chi^2 = 715$ (591 dof). The set of best-fit values of temperatures (MK) and emission measures ($10^{52}$ cm$^{-3}$) are 20.9±1.0, 8.7±0.6, 4.9±0.3, 0.04±0.02 and 3.03±0.25, 2.18±0.39, 2.37±0.44, 0.05±0.02, respectively, while the best-fit interstellar hydrogen column density is $N_{\rm H} = (2.0 \pm 0.5)\ 10^{18}$ cm$^{-2}$. The weak coolest component serves only to formally fit the He II 304 Å line. If we force the temperature of the coolest component to be about the nominal formation temperature for He II, 0.01 keV, (as we do in the DEM analysis) we obtain $\chi^2 = 721$ with an emission measure 0.07 for the coolest component and the other parameters unchanged.

Fig. 3 shows the fit residuals. Though the fit is significantly improved and nearly acceptable, there remains a problem at ∼1.2 keV which probably reflects the incompleteness of the Fe L spectral model. Figures 4 and 5 give the spectra and the best-fit models. The EUVE SW spectrum shows the six prominent lines of Fe XVIII up to Fe XXIII at wavelengths of 93.9, 108.4, 121.8, 128.7, 135.8, and 132.85 Å, respectively. The ASCA spectrum shows prominent features from the He- and H-like lines complexes from Ne, Si, S, and Ar at about 1, 1.9, 2.5, and 3.2 keV, respectively.

Table 1 presents the resulting coronal abundances relative to the Anders and Grevesse (1989) solar photospheric values. All well-constrained abundances are significantly below solar except for that of Ne. We note that Vilhu et al. (1987) measured the photospheric “metal” abundance of AB Dor and found this to be solar. The coronal abundances of the poorly–constrained elements are consistent with reduced abundances or (in the case of Ar and Ca) also with solar abundances. However, the nitrogen abundance cannot be constrained by ASCA because of calibration problems below 0.6 keV (S.A. Drake, private communication). The quoted errors are rms errors derived from the $\chi^2$+2 criterion corresponding to 1$\sigma$-confidence contours for one interesting parameter. Note that these are not equal to the 68% confidence contours since the corresponding stochastic variable has a $\chi^2$-distribution of one degree of freedom.

We fix the abundances at the values given in Table 1 and use the best-fit value of $N_{\rm H}$ throughout all following DEM analyses. The DEM analysis with the regularization method now gives a much better fit ($\chi^2$ = 706 for 579 dof) than the corresponding fit with solar abundances ($\chi^2$ = 1284, cf. Sec. 5.1.). The resulting temperature structure and the goodness of the fit are comparable to those of the 4-T fit. The DEM (Fig. 6) no longer shows statistically significant negative excursions, suggesting that this model is more realistic. The small DEM component just above $10^5$ K is needed to fit formally the prominent EUVE He II 304 Å line (cf. above).

The clean algorithm gives a somewhat poorer fit ($\chi^2$ = 771), probably because full convergence has not yet taken place. In keeping with the known properties of the two methods for deriving DEMs, the "clean" solution tends to concentrate the emission measure into narrow temperature regions, whereas the regularization method favors smooth distributions and produces a DEM with broader, shallower peaks (cf. discussion in Kaastra et al. 1996a). In both solutions the DEM shows two maxima in the temperature intervals 5–8 MK and 20–30 MK. However, there appears to be a significant difference between the two solutions in the hotter component: the "clean" solution is strongly weighted towards a lower temperature of 20 MK, while the regularization solution peaks at 30 MK. This difference presumably arises from the effect of the continuum in the EUVE SW spectrum on the solution method.

In fitting procedures such as this artefacts can be introduced by an inappropriate choice of the temperature range considered in the fitting process. We have investigated the effect of using a larger temperature interval (i.e. 0.001–100 keV in 51 steps) in determining the solutions with the regularization method (cf. Fig. 7). We find no significant contributions to the DEM outside the temperature range $10^5$–$10^8$ K except for the component at $\sim 4\ 10^4$ K, which is caused by the He II line. The narrower temperature range ($10^5$–$10^8$ K) restricts this component to the lower boundary of $10^5$ K (cf. Fig. 6). The quality of the fit is comparable to the previous one: $\chi^2$ = 699 for 559 dof. Assuming solar abundances for the larger temperature interval yields for the regularization method a strong hot component in the DEM between $10^8$ and $10^9$ K, which again is needed to compensate for the effect of the incorrect abundances on the line/continuum ratio in the EUVE SW spectrum, and is therefore unphysical.

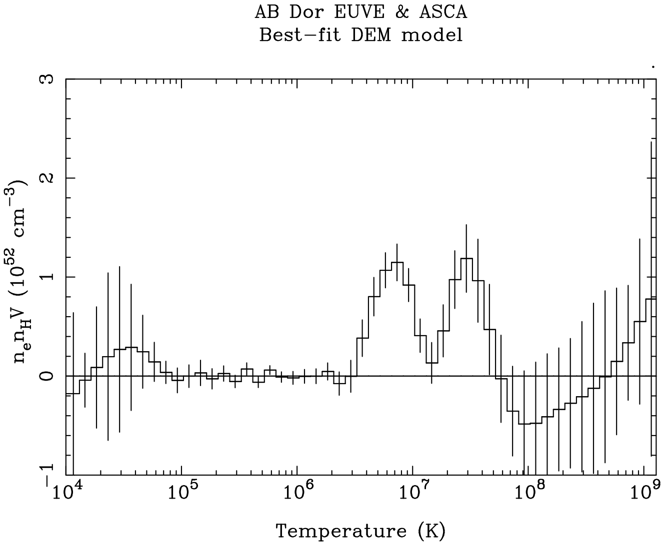


**Fig. 7.** The DEM for the combined EUVE & ASCA data using the regularization method with abundances from Table 1, but with a larger temperature interval.

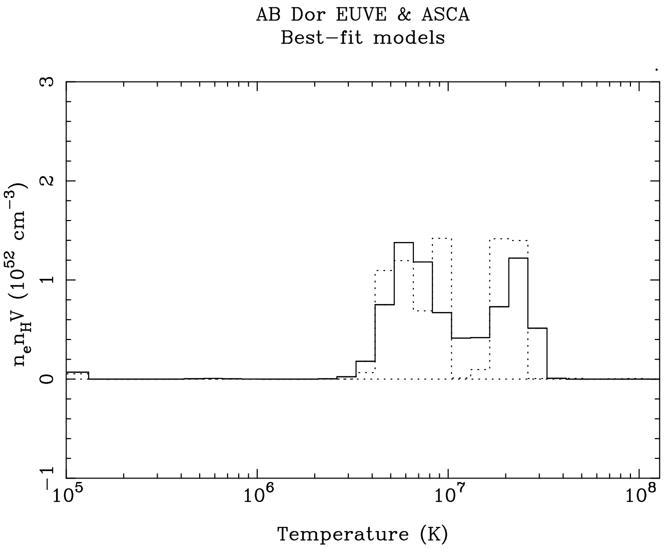


**Fig. 8.** The DEM for the combined EUVE & ASCA data using the polynomial method (solid line) or the genetic algorithm (dotted line) with abundances from Table 1.

For comparison we present in Fig. 8 the results obtained with the polynomial method and the genetic algorithm. In the statistical sense, these fits are of quality very similar to those of the regularization and clean methods: $\chi^2$ = 725 (600 dof) for the polynomial method with N=10 and $\chi^2$ = 730 (579 dof) for the genetic method. The results of the two methods are in good agreement and also with those of the previously used methods.

If we consider the instruments separately we find, as noted earlier, that ASCA gives the most stringent con-

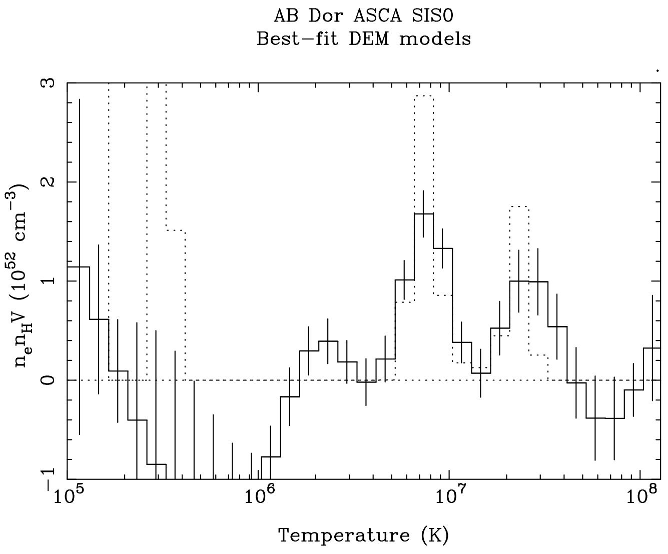


**Fig. 9.** The DEM for only the ASCA data using the regularization method (solid line with error bars) or the polynomial method (dotted line) with abundances from Table 1.

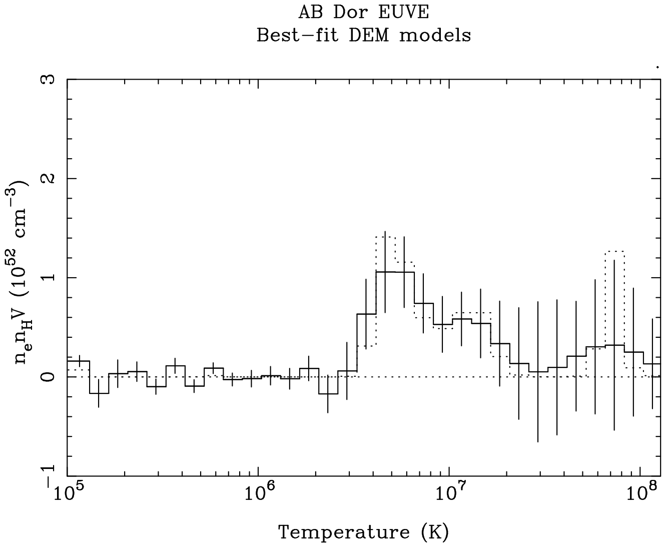


**Fig. 10.** The DEM for only the EUVE data using the regularization method (solid line with error bars) or the polynomial method (dotted line) with abundances from Table 1.

straint on the abundances, whereas with EUVE alone the abundances cannot be well determined. The combination of both instruments gives the best constraint.

For the ASCA data alone we have made a 3-T fit (a $4^{\rm th}$ cool component is not needed because there is no He II line). We vary all ten abundances, but keep the interstellar density constant at the previously derived value because ASCA alone gives no constraint on $N_{\rm H}$. We obtain a satisfactory fit with $\chi^2 = 152$ (131 dof). The derived abundances are all within at most $2\sigma$ of the abundances derived for the 4-T fit on the combined ASCA & EUVE data (Table 1) so that in the following DEM analyses we adopt the latter values again.

Fig. 9 gives the DEM for the ASCA SIS0 data with $\chi^2 = 151$ (116 dof) for the regularization method and $\chi^2 = 169$ (138 dof) for the polynomial method with N=9.

Fig. 10 gives the DEM for the EUVE data with $\chi^2 = 502$ (432 dof) for the regularization method and $\chi^2 = 514$ (449 dof) for the polynomial method with N=14. We note that here the regularization method does not show the strong "hot tail" as we have found earlier in fitting the EUVE data with a model with solar abundances (Rucinski et al. 1995). This indeed confirms our suggestion that a lower (than solar) Fe abundance is more realistic (cf. Rucinski et al. 1995).

It is clear that ASCA gives the strongest constraint on the DEM at high temperatures ($\gtrsim$ 6 MK), but virtually no constraint at very low temperatures ($\lesssim$ 1 MK) (see polynomial results in Fig. 9!). On the contrary, EUVE gives a better constraint at low temperatures ($\lesssim$ 6 MK), but no constraint at very high temperatures ($\gtrsim$ 10 MK) (see polynomial result in Fig. 10).

## 6. Discussion

We have fit simultaneously–obtained EUVE and ASCA spectra of the quiescent phase of the active K0–dwarf star AB Doradus to optically thin plasma models in order to determine the distribution of coronal emission measure with temperature. If we assume solar photospheric abundances for the coronal plasma, we do not find any satisfactory fits. If we allow the abundances to vary the fit improves significantly.

We have used four different DEM methods. Though there are differences between the solutions they all yield a qualitatively similar DEM distribution which is essentially bimodal with temperatures concentrated on the intervals 5–8 MK and 20–30 MK. This behaviour is similar to that found for the X-ray emission from Algols (Singh et al. 1995). We note that the fits are formally (i.e. in a $\chi^2$ sense) not acceptable. This reflects the fact that uncertainties in instrument calibration, atomic physics and deconvolution of the spectra, and insufficient spectral resolution, still continue to contribute systematic effects in determining DEMs.

Our most important result is the confirmation that non–solar abundances are required to model the spectra satisfactorily. Of the well constrained abundances Fe is underabundant by a factor of 3 while O, Mg, Si and S are underabundant by a factor of 2, whereas Ne may be slightly overabundant. Other ASCA spectra of RS CVn's such as AR Lac, Algol-type binaries, and single stars (for references for all these types of stars, e.g., White et al. 1994, Kaastra et al. 1996a, Singh et al. 1995, 1996, Antunes et al. 1994, Drake et al. 1994, 1996), have also uncovered a pattern in which the abundances of metals (e.g., Fe) appear to be *depleted*, rather than *enhanced* as they are in the solar corona for the elements with low FIP (e.g., Feldman 1992), by factors of up to $\sim$ 3–5 with respect to solar photospheric values. Evidence for an under-abundance of iron was also found from analyses of the EUVE spectra of Algol and AB Dor (Stern et al. 1995, Rucinski et al. 1995). The analysis of an EUVE SW spectrum of the RS CVn binary CF Tuc revealed an extreme case of a low coronal iron abundance of even 0.1 $\times$ solar (Schmitt et al. 1996a) leading to the introduction of the term "MAD" syndrome (metal abundance deficiency). However, the abundances derived from the EUVE spectra have been controversial because they rely on the interpretation of the ratio of strong Fe lines to an apparent continuum in the SW region of the spectrum, and competing explanations suggest that either the lines may be reduced by resonant scattering (Schrijver et al. 1994, 1995) or the apparent continuum level may be enhanced by a forest of weak unresolved (and unidentified) lines (Schmitt et al. 1996b, Mewe et al. 1996b). Both effects diminish the line–to–continuum ratio and make the Fe abundance low. However, neither effect is expected to play a role in the ASCA spectrum, which independently requires low abundances, though there continues to be doubt that the atomic physics in the vicinity of the Fe L–shell lines is thoroughly understood. Thus, while systematic effects may still play a role in this result, two independent spectra both appear to require an under-abundance of Fe. This effect, contrasting as it does with the overabundance of Fe in the solar corona, remains to be explained.

We conclude by pointing out again the great power of being able to deconvolve EUVE and ASCA spectra of the same object together. Because of the complementary strengths of the two wavelength ranges, their combination is a far more powerful tool than is either spectrum alone.

*Acknowledgements.* The Space Research Organization of the Netherlands (SRON) is supported financially by NWO, the Netherlands Organization for Scientific Research. SMW acknowledges the support of NASA grants NAG–52364 (EUVE) and NAG–52531 (ASCA) for this work, and thanks Rob Petre and the ASCA team for scheduling the ASCA AB Dor observation at short notice to coincide with the previously–scheduled EUVE observation. The work of RP has been supported by the Italian Space Agency (ASI).

## References

Anders E., Grevesse N. 1989, Geochimica et Cosmochimica Acta 53, 197
Antunes A., Nagase F., White N.E., 1994, ApJ 436, L83
Charbonneau P., 1995, ApJS 101, 309
Collier Cameron A.C., Bedford D.K., Rucinski S.M., Vilhu O., White N.E., 1988, MNRAS 231, 131
Collier Cameron G., Robinson R.D., 1989, MNRAS 236, 57
Drake S.A., Singh K.P., White N.E., Simon T., 1994, ApJ 436, L87
Drake S.A., Singh K.P., White N.E., 1996, in: Bowyer S., Malina R.F. (eds.) IAU Coll. 152, Astrophysics in the Extreme Ultraviolet, Kluwer Acad. Publ., Dordrecht–Holland, p. 147
Feldman U., 1992, Phys. Scripta 46, 202
Guirado J.C., Preston R.A., Jones D.L. et al., 1995, in: Paredes, J.M., Taylor, A.R. (eds.) Radio Emission from the Stars and the Sun, Astron. Soc. Pacific, San Francisco, in press
Högbom J.A., 1974, A&AS 15, 417
Innis J.L., Thompson K., Coates D.W., 1986, MNRAS 223, 183
Kaastra J.S., Mewe R., 1993, Legacy 3, 16
Kaastra J.S., Mewe R., Liedahl D.A., et al., 1996a, A&A, in press
Kaastra J.S., Mewe R., Nieuwenhuijzen H., 1996b, in: Watanabe T. (ed.) The 11th colloquium on UV and X-ray Spectroscopy of Astrophysical and Laboratory Plasmas, Universal Academy Press, Tokyo, in press
Kürster, M., 1995, in: Strassmeier K., Linsky J.L. (eds.) Stellar Surface Structure, in press
Kürster M., Dennerl K., 1993, in: Linsky J.L., Serio S. (eds.) Physics of Solar and Stellar Coronae, p. 443
Kürster M., Hatzes A.P., Pallavicini R., Randich S., 1992, in: Giampapa M.S., Bookbinder J.A. (eds.) 7th Cambridge Workshop on Cool Stars, Stellar Systems, and the Sun, p. 249
Kürster M., Schmitt J.H.M.M., Cutispoto G., 1994, A&A 289, 899
Landini M., Monsignori Fossi B.C., 1990, A&AS 82, 229
Lim J., Nelson G., Castro C., Kilkenney D., van Wyk F., 1992, ApJ 388, L27
Lemen J.R., Mewe R., Schrijver C.J., Fludra A., 1989, ApJ 341, 474
Liedahl D.A., Osterheld A.L., Goldstein W.H., 1995, ApJ 438, L115
Mewe R., Gronenschild E.H.B.M., van den Oord G.H.J., 1985, A&AS 62, 197
Mewe R., Kaastra J.S., 1994, European Astronomical Society Newsletter, Issue 8, June 1994, p. 3
Mewe R., Kaastra J.S., Liedahl D.A., 1995a, Legacy 6, 16
Mewe R., Kaastra J.S., Schrijver C.J., van den Oord G.H.J., Alkemade F.J.M., 1995b, A&A 296, 477
Mewe R., Kaastra J.S., White S.M., Pallavicini R., 1996a, in: Pallavicini R., Dupree A.K. (eds.) 9th Cambridge Workshop on Cool Stars, Stellar Systems, and the Sun, in press
Mewe R., Lemen J.R., van den Oord G.H.J., 1986, A&AS 65, 511
Mewe R., van den Oord G.H.J., Schrijver C.J., Kaastra J.S., 1996b, in: Bowyer S., Malina R.F. (eds.) IAU Coll. 152, Astrophysics in the Extreme Ultraviolet, Kluwer Acad. Publ., Dordrecht–Holland, p. 553
Meyer J., 1991, Adv. Space Res. 11, 1, 269
Morrison R., McCammon D., 1983, ApJ 270, 119
Pakull M.W., 1981, A&A 104, 3
Rucinski S.M., 1985, MNRAS 215, 591
Rucinski S.M., Mewe R., Kaastra J.S., Vilhu O., White S.M., 1995, ApJ 449, 900
Schmitt J.H.M.M., Drake J.J., Stern R.A., 1996b, submitted to ApJ
Schmitt J.H.M.M., Stern R.A., Drake J.J., Kürster M., 1996a, ApJ in press

Schrijver C.J., van den Oord G.H.J., Mewe R., 1994, A&A 289, L23

Schrijver C.J., Mewe R., van den Oord G.H.J., Kaastra J.S., 1995, A&A 302, 438

Singh K.P., Drake S.A., White N.E., 1995, ApJ 445, 840

Singh K.P., White N.E., Drake S.A., 1996, ApJ 456, 766

Stern R.A., Lemen J.R., Schmitt J.H.M.M., Pye J.P., 1995, ApJ 444, L45

Swank J.H., White N.E., Holt S.S., Becker R.H., 1981, ApJ 246, L149

Verner D.A., Yakovlev D.G., 1995, A&AS 109, 125

Vilhu O., Gustafsson B., Edvardsson B., 1987, ApJ 320, 850

Vilhu O., Tsuru T., Collier Cameron A., 1991, in: Treves A., Perola G.C., Stella L. (eds.) Iron Line Diagnostics in X-ray Sources, p. 30

White N.E., Arnaud K.A., Day C.S.R., et al., 1994, PASJ 46, L97

White N.E., 1996, in: Pallavicini R., Dupree A.K. (eds.) 9th Cambridge Workshop on Cool Stars, Stellar Systems, and the Sun, in press

White S.M., Lim J., Rucinski S., et al., 1996a, ApJ, in preparation

White S.M., Pallavicini R., Lim J., 1996b, in: Gershberg R., Greiner. J., Duerbeck H. (eds.) Flares and Flashes, in press

White S.M., Pallavicini R., Lim J., 1996c, in: Pallavicini R., Dupree A.K. (eds.) 9th Cambridge Workshop on Cool Stars, Stellar Systems, and the Sun, in press

This article was processed by the author using Springer-Verlag LaTeX A&A style file *L-AA* version 3.